Effect of the Interaction Length on Clusters Formed by Spherical One-Patch Particles on Flat Planes

メタデータ	言語: eng 出版者: 公開日: 2021-04-15 キーワード (Ja): キーワード (En): 作成者: メールアドレス: 所属:
URL	https://doi.org/10.24517/00061714

This work is licensed under a Creative Commons Attribution-NonCommercial-ShareAlike 3.0 International License.

Effect of Interaction Length on Clusters formed by Spherical One-Patch Particles on Flat Planes

Masahide Sato*

Information Media Center, Kanazawa University, Kanazawa 920-1192, Japan

E-mail: msato002@staff.kanazawa-u.ac.jp

Abstract

Considering that one-patch particles rotate three-dimensionally and translate on a two-dimensional flat plane, I perform isothermal-isochoric Monte Carlo simulations to study how two-dimensional self-assemblies formed by spherical patchy particles depend on the interaction length and patch area. As the interaction potential between one-patch particles, the Kern-Frenkel (KF) potential is used in the simulations. With increasing the patch area, the shape of the most numerous clusters changes from dimers to island-like clusters with a square lattice via triangular trimers, square tetramers, and chain-like clusters when the interaction length is as long as the particle radius. With a longer interaction length, other shapes of polygonal clusters such as another type of square tetramers, two types of pentagonal pentamers, hexagonal hexamers, and hexagonal heptamers also form.

Introduction

Particles having patch areas, whose properties are different from those of the other surface area, are termed patchy particles. They are promising building blocks for functional materials because unique and complicated structures that are not created with isotropic particles form owing to the anisotropic interaction induced by the patch areas. For example, the triblock patchy particles which have two patches on their polar positions are considered to be used building blocks for photonic crystals with complete photonic band gap.[1–4] Many groups[3–40] have studied self-assemblies formed by patchy particles. Preisler et al.[26] used the Kern-Frenkel (KF) potential[44] and performed Monte Carlo simulations for one-patchy particles with a short interaction length. They showed that close packed structures with complicated bondings are created by controlling the coverage of the patch area.[24] They also examined how the three-dimensional structures formed by Janus particles depend on the interaction length and showed that various types of open structures, which are not created with short interaction lengths, are created with long interaction lengths.[26] In the study, the patch area was set to be the half of the whole surface. In addition, the interaction lengths were shorter than the half of the particle diameter. Thus, it remains as an interesting problem to study which kinds of new structures are created when the ratio of the patch area changes with much longer interaction lengths.

The formation of two-dimensional materials with a single layer thickness becomes a popular topic because the two-dimensional materials are used for broad applications such as photovoltaics, semiconductors, electrodes and water purification.[42,43] To create quality two-dimensional structures are also beneficial because these films can be used as substrates for colloidal epitaxy.[47–49] It is hard to create quality three-dimensional functional materials in the free three-dimensional space spontaneously, but it might be easy to create desired structures on substrates by epitaxial growth. To create quality substrates formed by patchy particles, it is important to understand how two-dimensional structures depend on the patch area and interaction length. Thus, I focus on studying the two-dimensional structures.

In this paper, assuming that one-patch particles with rotating three-dimensionally translate on flat planes, I perform isothermal-isochoric Monte Carlo simulations to examine how two-dimensional self-assemblies change with the strength of interaction energy, the patch area, and the density of patchy particles. In previous studies,[45,46] I performed isothermal-isobaric Monte Carlo simulations and studied the dependence of structures on the patch area in two-dimensional systems and thin systems, where the interaction length is fixed at the half of the diameter of particles. Here, I focus on the systems, where the interaction length is equal to or longer than the half of the diameter. First, I introduce the model used in my simulations. In this study, the Kern-Frenkel potential is used as the potential between patchy particles. Next, I show the results of my simulations. In previous papers,[3,4] it was reported that the two-step process, in which colloidal crystal form via the formation of colloidal molecules, is useful to create complicated structures. it was also suggested that the formation of clusters with uniform size and shape is important to create quality structures.[3,4] Thus, after showing several snapshots of typical clusters, I study how the distribution of cluster types changes with the patch area. I also examine the dependence of the shape of most numerous cluster on parameters such as the interaction length, the interaction range, the interaction energy, and the particle density. Lastly, I summarize my results in conclusions.

Methods

It is assumed that spherical patchy particles rotating three-dimensionally translate on a flat plane. The particles interact with the KF potential.[44] The interaction potential between the ith and jth particles, $U^{\mathrm{KF}}(r_{ij})$, is expressed as

$$U^{\mathrm{KF}}(r_{ij}) = U_{\mathrm{rep}}(r_{ij}) + U_{\mathrm{att}}(r_{ij}) f(\hat{\boldsymbol{r}}_{ij}, \hat{\boldsymbol{n}}_i, \hat{\boldsymbol{n}}_j), \tag{1}$$

where $\boldsymbol{r}_i$ represents the position of the center of the ith particle, $\boldsymbol{r}_{ij} = \boldsymbol{r}_j - \boldsymbol{r}_i$, $r_{ij} = |\boldsymbol{r}_{ij}|$, $\hat{\boldsymbol{r}}_{ij} = \boldsymbol{r}_{ij}/r_{ij}$, and $\hat{\boldsymbol{n}}_i$ indicates the patch direction of the ith particle. The first term in

Eq. (1) represents the hard-core repulsive potential given by

$$U_{\rm rep}(r_{ij}) = \begin{cases} \infty & (r_{ij} \leq \sigma) \\ 0 & (\sigma < r_{ij}) \end{cases}, \tag{2}$$

where σ is the diameter of spherical patchy particles and set to unity. The second term in Eq. (1) is the attractive part in the KF potential. $U_{\rm att}(r_{ij})$ is the square-well potential given by

$$U_{\rm att}(r_{ij}) = \begin{cases} -\epsilon & (\sigma < r_{ij} \leq \sigma + \Delta) \\ 0 & (\sigma + \Delta < r_{ij}) \end{cases}, \tag{3}$$

where ϵ represents the strength of attraction and Δ is the interaction length. $f(\boldsymbol{r}_{ij}, \hat{\boldsymbol{n}}_i, \hat{\boldsymbol{n}}_j)$ represents the anisotropy in the attraction, which is given by

$$f(\hat{\boldsymbol{r}_{ij}}, \hat{\boldsymbol{n}}_i, \hat{\boldsymbol{n}}_j) = \begin{cases} 1 & (\hat{\boldsymbol{n}}_i \cdot \hat{\boldsymbol{r}}_{ij} > \cos\theta \text{ and } \hat{\boldsymbol{n}}_j \cdot \hat{\boldsymbol{r}}_{ji} > \cos\theta\ ) \\ 0 & \text{otherwise} \end{cases}. \tag{4}$$

Since the diameter of the patchy particles is given by σ, the patch area S is estimated as $\pi\sigma^2(1-\cos\theta)/2$. The relationship between θ and the ratio of the patch area to the whole surface area, χ, is given by $(1-\cos\theta)/2$. θ changes from 20° and 100° in my simulations. Thus, χ changes from 3.0×10^{-2} to 5.9×10^{-1}.

I study systems with long interaction lengths. In my previous studies,[45,46] I examined the structures formed in isothermal-isobaric systems for $\Delta/\sigma = 0.5$ and showed that structures which are not observed in systems with short interaction lengths are created. Here, I study the possibility of the formation of various clusters for $\Delta/\sigma \geq 0.5$. Recently, DNA guided crystallization has been studied,[50–68] and various types of lattice structures were created. In several studies,[38,40] the DNA strands are used as the source of the attractive interaction of patchy particles. The KF interaction with long Δ might be realized by the attraction caused by DNA strands because flexible and desired DNA strands are synthesized freely

now. However, the effects of steric hindrance should not be neglected when Δ/σ is too long. For example, for large clusters such as heptemers I show later in this paper, DNA strands have trouble bonding to the diagonal particle because another particle sets exactly between the two particles. Since the DNA strands have to curve around the intermediate particle, the significant entropic cost is necessary and the interaction range are effective reduced. Thus, the cases that Δ is as long as σ should be considered carefully.

Results and discussions

Square systems whose size is given by $L \times L$ with the periodic boundary conditions are considered. When the number of particles is N and the area fraction of system is ϕ, L is given by $(N\pi\sigma^2/4\phi)^{1/2}$. In my simulations, N and ϕ are mainly set to 2048 and 0.2, respectively. Initially, particles are put in the system at random. Then, their translation and rotation are performed for every particle. In a Monte Carlo (MC) trial, both translation and rotation are tried for a particle. At least 8×10^6 MC trials are performed per particle. To avid making the success rate of MC trials too low, the amplitude of both translation and rotation is tuned every $100N$ MC trials. The interaction strength used in my simulations is set to be equal to or less than $\epsilon/k_{\mathrm{B}}T = 8.0$, which is about as large as the he interaction strength reported in the experimental study.[16] The interaction strength is feasible and the clusters obtained in our simulations can be created experimentally when the interaction potential like the KF potential with long interaction is realized.

Clusters forming with $\Delta/\sigma = 0.5$

First, the dependence of cluster types on θ is examined for $\Delta = 0.5\sigma$. Figure 1(a)-(f) show snapshots of systems for several θ with $\epsilon/k_{\mathrm{B}}T = 8.0$. The zoomed snapshots of the clusters indicated by (A), (B), (C), (D), (E), and (F) in Figure 1(a)-(f) are shown in Figure 1(g). The snapshots where interacting particles are connected with yellow lines are also shown

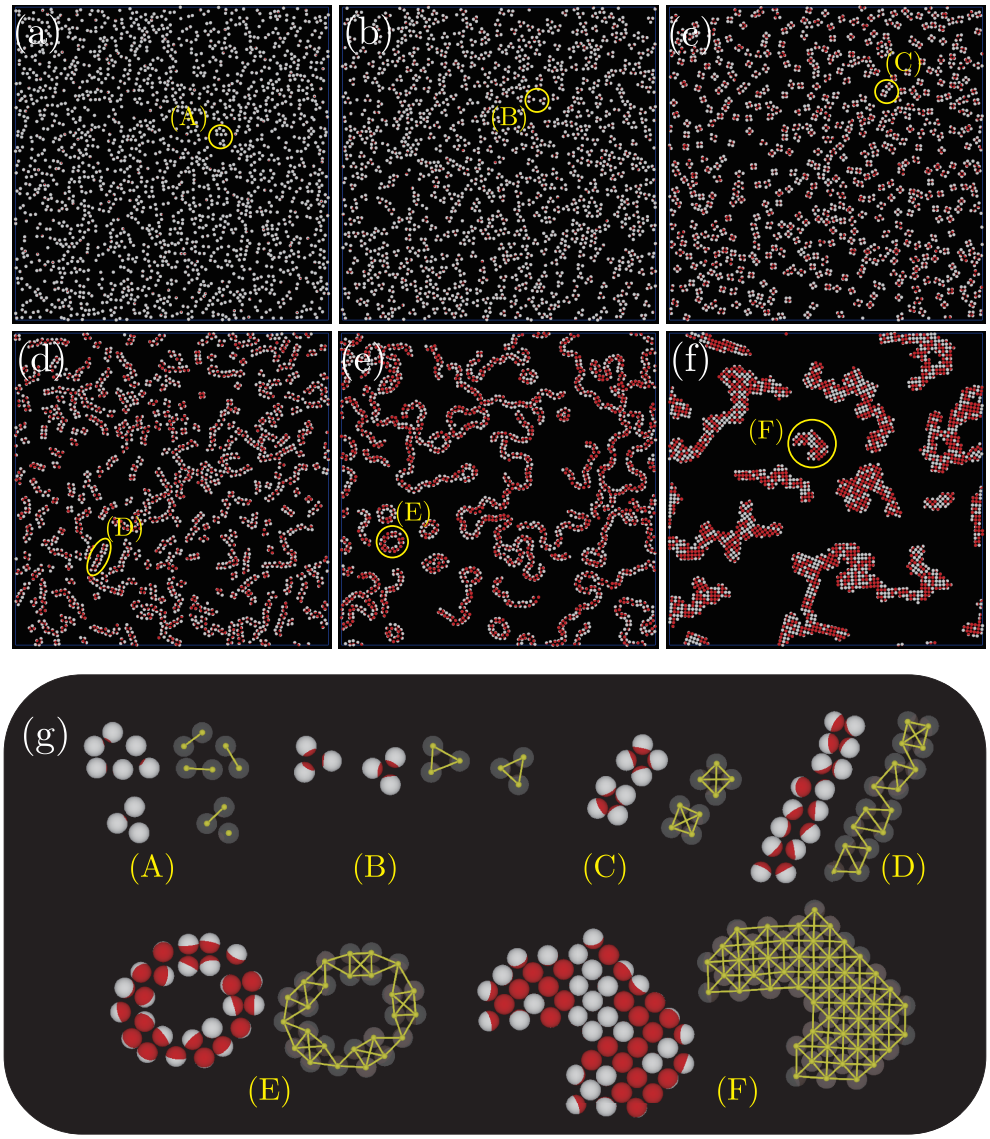

Figure 1: (a)-(f) snapshots of clusters for $\Delta/\sigma = 0.5$ and (g) clusters indicated as (A), (B), (C), (D), (E), and (F) in (a)-(f). Attractive interactions in the clusters, where the interacting particles are connected by yellow lines, are also shown. For the snapshots, $\phi = 0.2$, $N = 2048$, and $\epsilon/k_{\mathrm{B}}T = 8.0$. θ is (a) 25°, (b) 45°, (c) 65°, (d) 75°, (e) 90°, and (f) 95°. In these figures, red regions of particles represent patch areas.

in Figure 1(g). When $\theta = 25°$ [Figure 1(a)], particles seem to be distributed randomly. In region (A) surrounded by yellow circle, eight particles form four dimers, and one particle remains as a monomer. Monomers and dimers seem to be dominant with this angle. When $\theta = 45°$ [Figure 1(b)] and 65°[Figure 1(c)], the shapes of the most numerous clusters become more obvious than that in Figure 1(a); many triangular trimers such as (B) and square tetramers such as (C) are created, respectively. Since Δ is set to be longer than $(\sqrt{2}-1)\sigma$, it is possible that the particles at the diagonal positions interact with each other in the square tetramers. Thus, in cluster (C), each particle in the square tetramers connects with the other three particles, which are the two neighboring particles and the particle in the diagonal position. When $\theta = 75°$ [Figure 1(d)], small clusters connect and short straight string-like clusters such as (D) form. In cluster (D), one square tetramer at the upper edge and three rhombic tetramers are connected. In the rhombic tetramers, the particles in the long diagonal positions do not connect with each other. Instead, these particles connect with a particle in the neighboring tetramer. When $\theta = 90°$ [Figure 1(e)], string-like clusters become longer and more meandering than those for $\theta = 75°$. Small double rings such as (E) in Figure 1(e) are also observed. The double ring-like cluster is created by the connection of square tetramers via one particle. When $\theta = 95°$ [Figure 1(f)], crystallization occurs and island-like clusters such as (F) are created. The patch directions of almost all the particles in the island-like clusters are approximately perpendicular to the plane. The compact island-like clusters consist of the square lattice and the particles inside the island-like clusters have eight connections, which are four connections with the nearest neighbors and four connections with the second nearest neighbors in the diagonal positions, no matter whether the patch direction of each particle is toward or against the wall. In our simulations, coalescence of large island-like clusters is very slowly because we used a simple algorithm. Probably, larger island-like clusters appear if much longer simulations are performed.

Figure 2 shows the distribution of cluster size [Figure 2(a)] and the dependence of the cluster numbers on θ for small clusters [Figure 2(b)]. In Figure 2(a), the color strength is

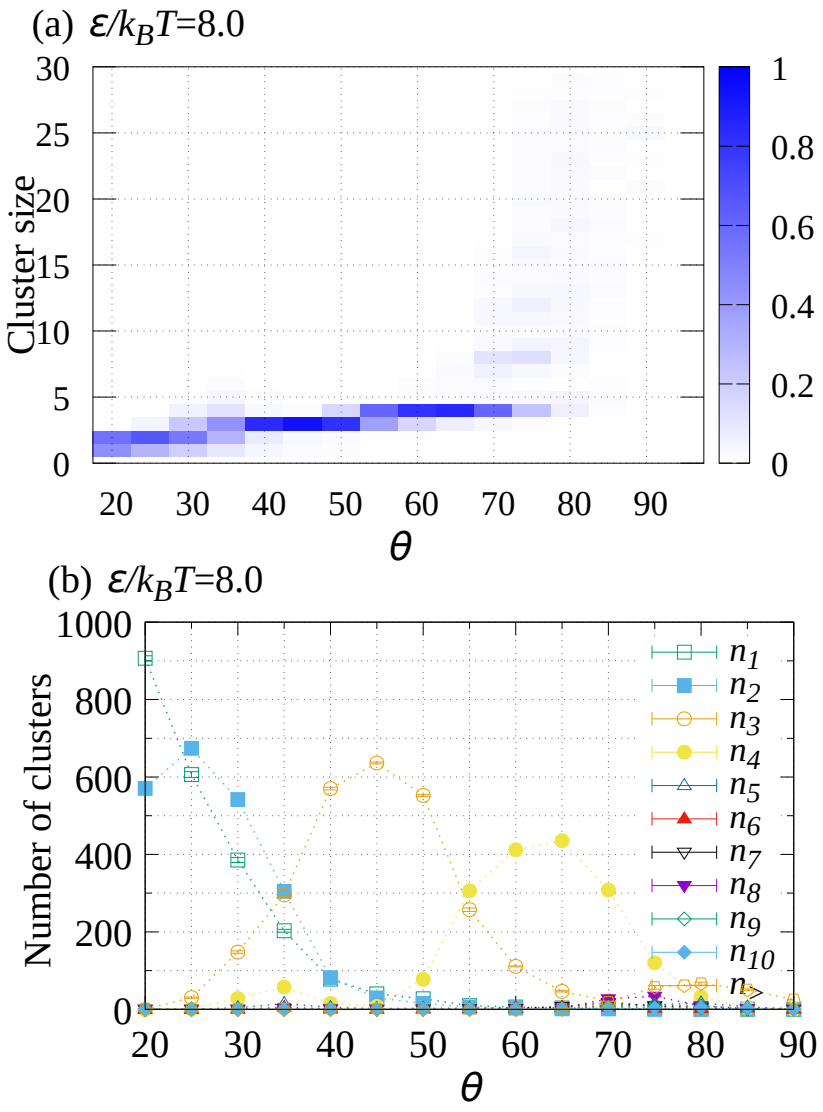

Figure 2: (a) Distribution of cluster size and (b) dependence of numbers of small clusters on θ for $\Delta/\sigma = 0.5$, where $\epsilon/k_{\rm B}T$ and ϕ are set to 8 and 0.2, respectively. The data in a single run are averaged over ten points every $2N \times 10^5$ MC step from $6N \times 10^6$ to $8N \times 10^6$.

proportional to kn_k/N, where n_k means the total number of the cluster whose size is k. When $\theta < 75°$, the cluster sizes are small for almost all the clusters, and the distribution of the cluster size is narrow. The cluster size of the most numerous cluster increases gradually with increasing θ. When θ exceeds 75°, large clusters start to be created and the distribution of cluster size becomes broader than that for $\theta < 75°$, which is consistent of the formation of sting-like clusters shown in Figure 1(d). Clusters consisting of less than 30 particles are rarely created when $\theta = 95°$, which is because many particles gather and large island-like clusters form as shown in Figure 1(f). The dependence of n_k on θ for small clusters is shown in Figure 2(b). When $\theta \leq 35°$, there are mainly dimers and monomers in the system. Trimers are dominant when $35° < \theta < 55°$, and tetramers are the most numerous cluster when $55° \leq \theta \leq 75°$. When $75° \leq \theta$, a few number of clusters consisting of more than ten particles are created, which indicates that long chain-like clusters and large island-like clusters form.

Dependence of cluster shapes on Δ

Here, I examine which types of clusters form when $\Delta/\sigma > 0.5$. After showing several typical snapshots, effects of θ and Δ/σ on the cluster type are studied.

Formation of another type of square tetramers. Clusters which are not created with $\Delta/\sigma = 0.5$ form when $\Delta/\sigma > 0.5$. Cluster (A) in Figure 3(a) shows another type of square tetramer observed with $\Delta/\sigma = 0.8$. Hereafter, this type of cluster is called tetramer (I). The connections of particles in tetramers (I) are different from those in the square tetramers created with $\Delta/\sigma = 0.5$ and $\theta = 75°$ [Cluster (C) in Figure 1(c), which I call tetramer (II)]. While particles in tetramers (II) connect with all the other particles in the same clusters, particles in tetramers (I) have only two connections with other two particles. Since θ is small, the particles cannot connect with both two nearest neighbors. Each particle just connects with one of the two nearest neighbors and the particle in the diagonal position.

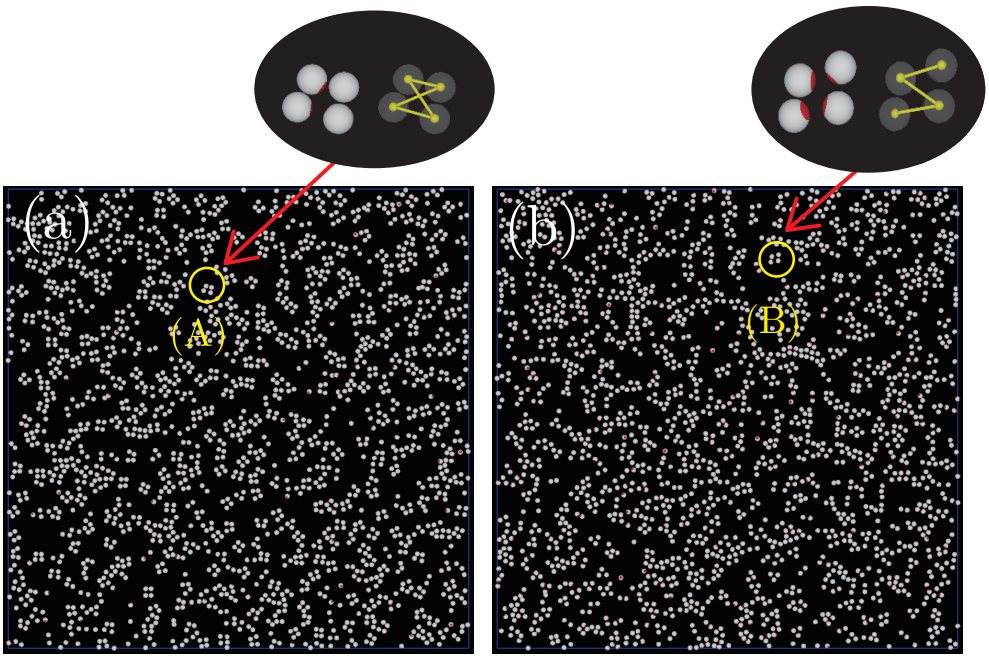

Figure 3: Snapshots of systems and zoomed snapshots of clusters, where $\phi = 0.2$, $N = 2048$, and $\epsilon/k_{\mathrm{B}}T = 8.0$. Δ/σ and θ is (a) 0.8 and 30° and (b) 0.5 and 35°.

As a reference, a tetramer formed with $\theta = 35°$ and $\Delta/\sigma = 0.5$ are shown as cluster (B) in Figure 3(b). It looks like a tetragonal tetramer, but the cluster is actually a zigzag chain-like cluster. A few tetramers were observed in Figure 2(b), but almost all the tetramers were this type of cluster.

Formation of pentamers, hexamers, and heptamers. Polygonal clusters which are larger than tetramers also form when $\Delta/\sigma > 0.5$. Figure 4 shows snapshots of systems with numerous pentamers, hexamers, and heptamers. The pentamers such as cluster (A) in Figure 4(a), which I call pentamers (I), are created with $\Delta/\sigma = 0.8$ and $\theta = 45°$. Not all particles interact with their nearest neighbors in pentamer (I) because θ is small. On the other hand, in the pentamer observed with $\Delta/\sigma = 0.8$ and $\theta = 45°$ such as cluster (B) in Figure 4(b), which I call pentamer (II), all the neighboring particles connect with each other because θ is sufficiently large. Hexamers such as cluster (C) and heptamers such as cluster (D) form when $\Delta/\sigma = 1.0$ and $\theta = 70°$ [Figure 4(c)]. There is a vacancy in which one particle can be placed at the center of the hexagonal hexamers. Since Δ/σ is just unity, the

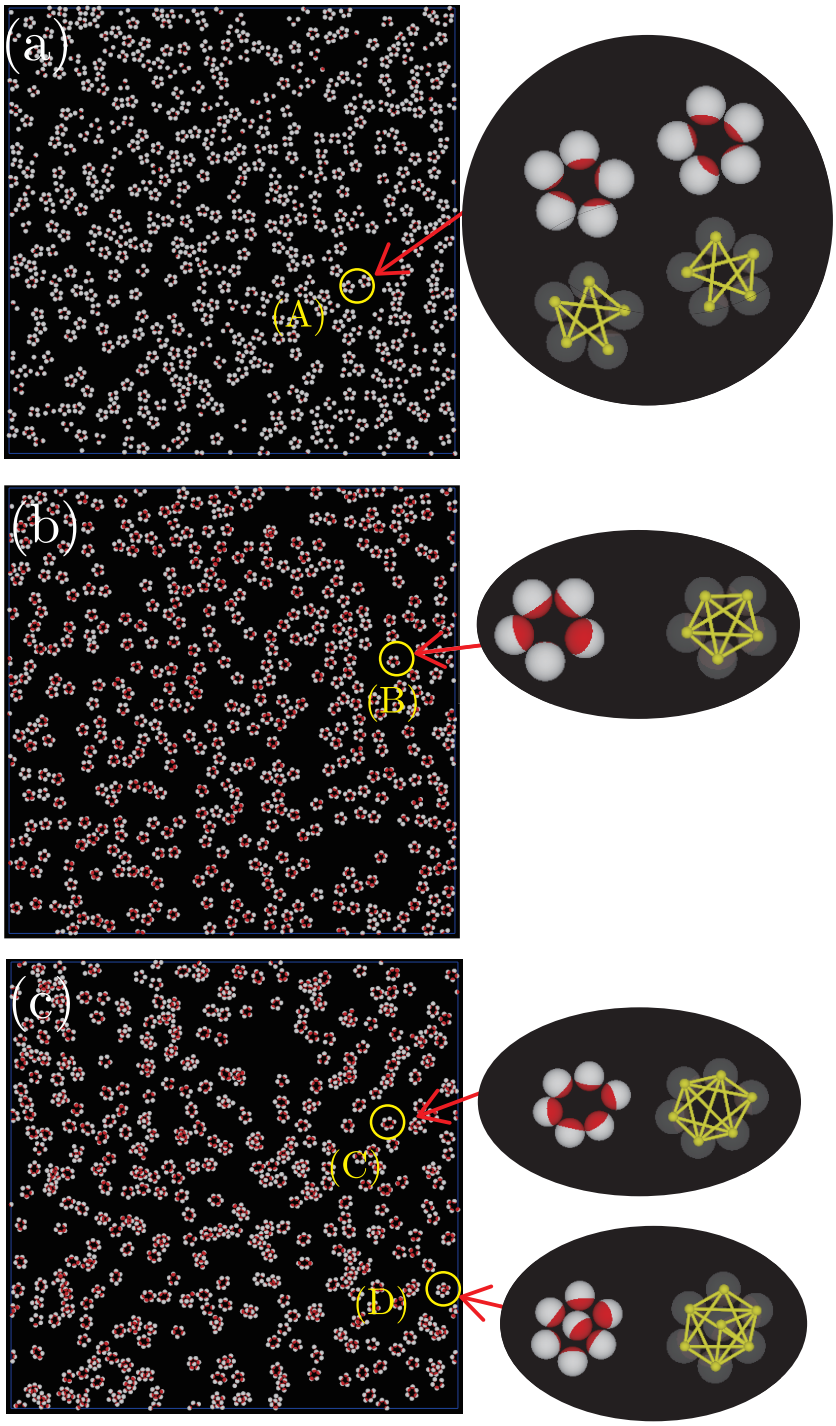

Figure 4: Snapshots of systems and zoomed snapshots of clusters, where $\phi = 0.2$, $N = 2048$, and $\epsilon/k_{\mathrm{B}}T = 8.0$; Δ/σ and θ are (a) 0.8 and 45°, (b) 0.8 and 70°, and (c) 1.0 and 70°.

connections between particles in diagonal positions in the ring-shaped hexamers are easily broken by thermal fluctuations. That is why one connection between particles in a diagonal position is broken in cluster (C). Its shape seems to be a bit deformed from the regular hexagonal hexamer. Heptamers such as (D) were also created when the central vacancies of ring-shaped hexamers are occupied by particles, but regular polygonal clusters which are larger than the heptamers were not observed in my simulations.

Effects of Δ/σ on chain-like clusters and island-like clusters. The same types of clusters forming with $\Delta/\sigma = 0.5$ are created when $\Delta/\sigma = 0.6$. The shapes of small polygonal clusters are hardly affected by the difference in Δ/σ, but chain-like clusters become more straight as shown in Figure 5, which is probably because the square tetramers with $\Delta/\sigma = 0.6$ are more stable against thermal fluctuations than those with $\Delta/\sigma = 0.5$. Since the interaction length is much longer than $(\sqrt{2}-1)\sigma$, the square tetramers can keep the interactions between particles even if their shapes are a bit warped. For $\theta = 75°$, the square tetramers seem to be the growth unit of chain-like clusters [Figure 5(a)], which is similar to the cooperative assembly.[38] Figure 5(c) shows the relationship between the number of clusters and the cluster size for $\theta = 75°$ and $\Delta/\sigma = 0.6$. The number of clusters is large when cluster sizes are the multiples of four, which supports that the growth unit of the double chain-clusters observed in Figure 5 is the square tetramer. For $\theta = 90°$ [Figure 5(b)], double rings and loops are observed, but their shapes are stiffer than those in Figure 1(e).

When Δ/σ is long enough for pentagonal pentamers to form, the shapes of chain-like clusters and island-like clusters are different from those obtained with $\Delta/\sigma = 0.5$. The growth unit of chain-like clusters changes from the square tetramer to the pentagonal pentamer. Chain-like clusters form by the connection of pentagonal pentamers as shown in (A) in Figure 6(a). The structure in island-like clusters also changes. For $\Delta/\sigma = 0.5$, the structure inside island-like clusters is the square lattice, and the peripheries of the clusters consist of facets as shown in the cluster (F) in Figure 1(g). However, the structure becomes

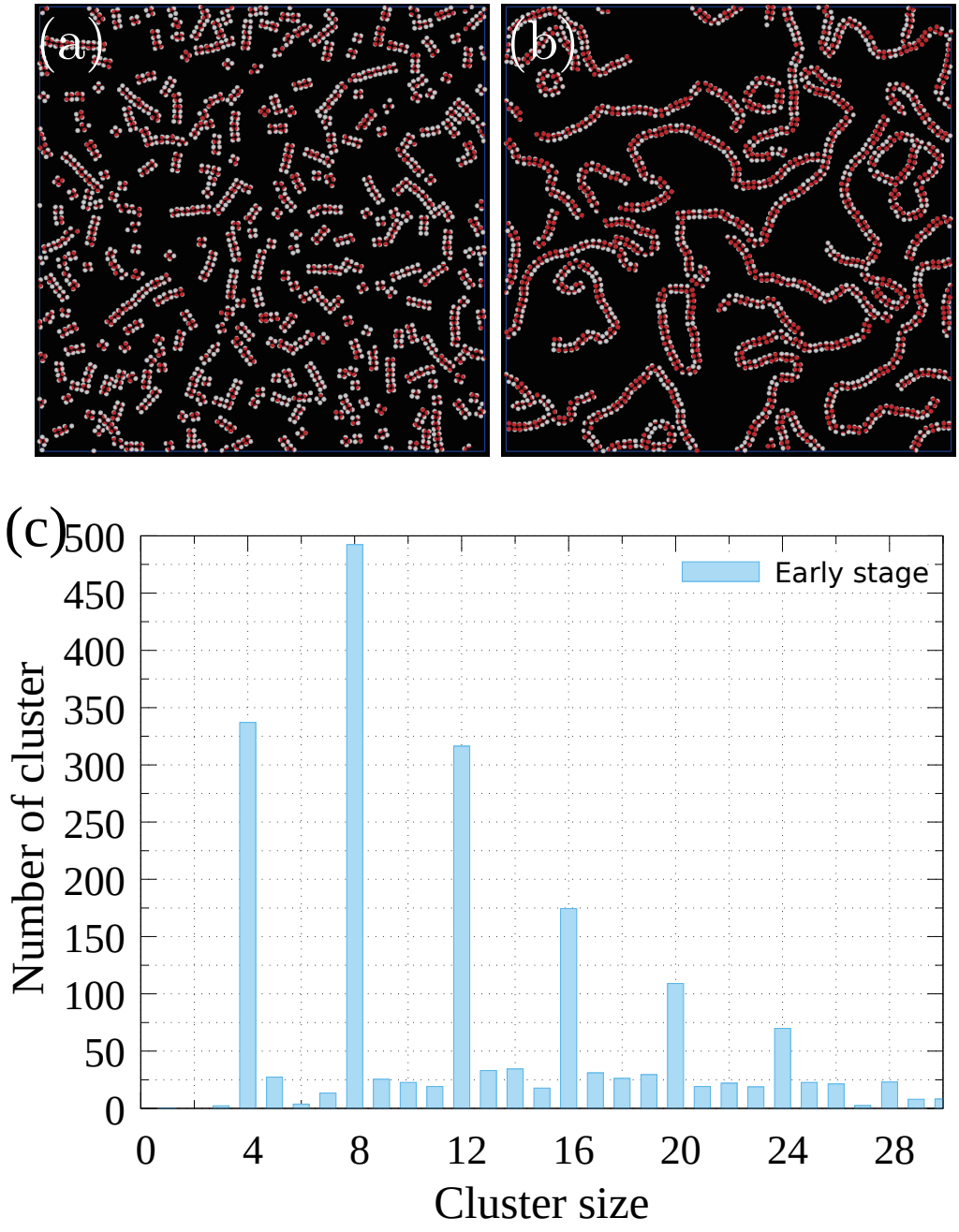

Figure 5: (a) and (b) snapshots of systems for $\Delta/\sigma = 0.6$, and (c) relationship between the number of clusters and the cluster size for $\theta = 75°$ and $\Delta/\sigma = 0.6$. In snapshots (a) and (b), $\phi = 0.2$, $N = 2048$, and $\epsilon/k_{\mathrm{B}}T = 8.0$. θ is (a) 75° and (b) 90°. In these figures, red regions of particles represent patch areas. In (c) The data are averaged over 10 points every $2N \times 10^5$ Monte Carlo steps from $6N \times 10^6$ Monte Carlo steps to $8N \times 10^6$ Monte Carlo steps.

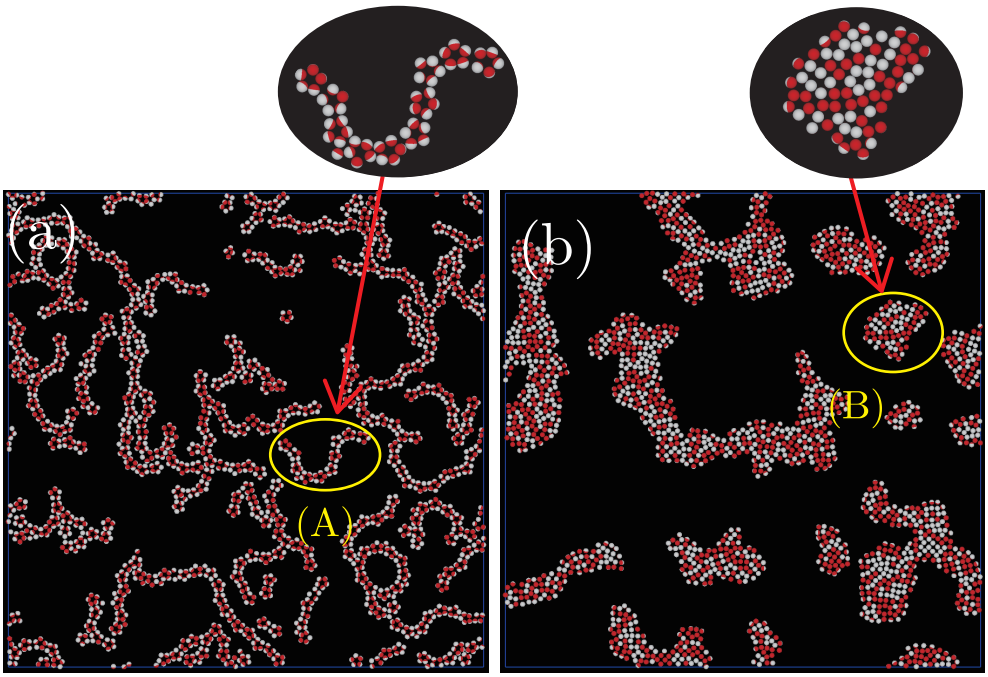

Figure 6: Snapshots of systems and zoomed snapshots of clusters, where $\phi = 0.2$, $N = 2048$, and $\epsilon/k_{\mathrm{B}}T = 8.0$. θ and Δ/σ are (a) 85° and 0.8 and (b) 95° and 0.7.

disorder and seems to consist of the mixture of square tetramers and pentagonal pentamers when $\Delta/\sigma = 0.7$ as shown in Figure 6(b).

Dependence of the type of the most numerous cluster on Δ/σ and θ. For $\phi = 0.2$ and $\epsilon/k_{\mathrm{B}}T = 8.0$, the dependence of the type of the most numerous cluster on θ and Δ/σ is shown in Figure 7(a). In Figure 2(b), the number of tetramers n_4 is larger than the sum of the numbers of clusters consisting of more than 10 particles when $\theta = 75°$. However, the total number of particles in chain-like clusters is more numerous than that in tetramers because the size of chain-like clusters is sufficiently larger than that of tetramers. Thus, $(\Delta/\sigma, \theta) = (0.5, 75°)$ is classified in the region of chain-like clusters in Figure 7(a).

Ideal shapes of several polygonal clusters we observed in our simulations are shown in Figure 7(b). When the patch directions of all particles are set to parallel to the plane where the particles are placed, the numbers of connections between particles are maximum for small polygonal clusters. Thus, the patch directions in the clusters in Figure 7(b) are assumed to be parallel to the plane. When θ is sufficiently small, the clusters shown in Figure 7(b) are

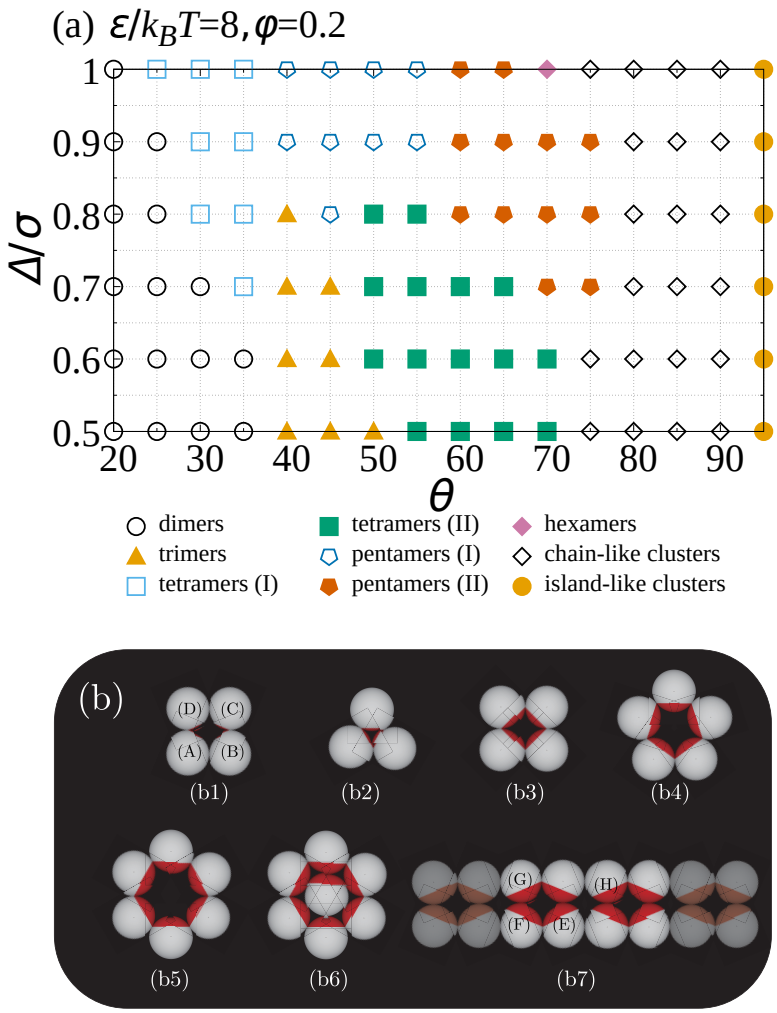

Figure 7: (a) Dependence of the type of the most numerous cluster on θ and Δ, where $\phi = 0.2$ and $\epsilon/k_{\mathrm{B}}T = 8.0$, and (b) Shapes of ideal clusters created with the minimum Δ/σ; (b1) square tetramer (I), (b2) trimer, (b3) square tetramer (II), (b4) pentagonal pentamer (II), (b5) hexagonal hexamer, (b6) hexagonal hepamer, and (b7) chain-like cluster formed with squares. In these clusters, the patch direction is assumed to be parallel to the plane where particles are placed, and θ are set to the minimum values for creating these clusters; (b1) 22.5°, (b2) 30°, (b3) 45°, (b4) 54°, (b5) 60°, (b6) 60°, and (b7) 67.5°

not created. The dimer is the most numerous cluster in the small θ region. The interaction energy change per particle by forming a dimer, u_2, is estimated to $-\epsilon/2$. The dimers can be created even when the interaction length is very short if the interaction is strong. When θ increases, the formation of larger clusters becomes possible. In square tetramers (I) [(b1) in Figure 7(b)], particles do not interact with one of the nearest neighbors. For example, particle (A) interacts with particles (C) and (B) but does not interact with particle (D). Thus, θ necessary for creating square tetramers (I) is given by 22.5° when $\Delta/\sigma = (\sqrt{2}-1) = 0.414$, which is the minimum interaction length for creating the tetramers. The minimum Δ for creating the regular triangular trimers [(b2) in Figure 7(b)] is smaller than that for square tetramers (I). Like the formation of dimers, the regular triangular trimers can be created with vary short interaction lengths. With the minimum interaction length, θ should be larger than 30° for the timers. Thus, the minimum θ is larger than the minimum θ for creating square tetramers (I). When the ideal regular trimers are created, the recovered connections per particle are two, which are the same as those for ideal square tetramers (I). The interaction energy change per particle by creating a trimer u_3 and that by creating a square tetramer (I) $u_{4(\mathrm{I})}$ are both estimated to $-\epsilon$. Taking into account thermal fluctuations, criteria on θ for creating these two clusters seem to be satisfied in Figure 7 because square tetramers (I) and trimers are the most numerous clusters when $25° \leq \theta$ and $40° \leq \theta$, respectively. Since dimers and trimers can be created even with a very short interaction length,[22,25,31] these clusters are more stable more than tetramers for the fluctuation of interparticle distance. Thus, the dimers and trimers become the most numerous clusters in small Δ/σ region in Figure 7.

The minimum Δ/σ necessary to create other ideal regular clusters and the minimum θ with the minimum Δ/σ are $(\sqrt{2}-1)$ and 45° for a square tetramer (II) [(b3) in Figure 7(b)], 54° and $(2\sin 54° - 1)$ for a pentagonal pentamer (II) [(b4) in Figure 7(b)], and unity and 60° for a hexagonal hexamer [(b5) in Figure 7(b)]. For pentagonal pentamers (I) with the minimum Δ/σ, the minimum θ is 18° if all the neighboring particles are not connected. The minimum Δ/σ is the same, but the minimum θ is much smaller than that of pentagonal

pentamers (II). Thus, the parameter regions where these clusters become dominant satisfy the criteria about θ and Δ/σ in Figure 7. The interaction energy changes per particle by creating these clusters are estimated to $u_{4(\mathrm{II})} = -3\epsilon/2$ for square tetramers (II), $u_{5(\mathrm{I})} = -\epsilon$ for pentagonal pentamers (I), $u_{5(\mathrm{II})} = -2\epsilon$ for pentagonal pentamers (II), and $u_6 = -5\epsilon/2$ for hexagonal hexamers. If all the particles in a pentagonal pentamer (I) do not interact with their two nearest neighbors, $|u_{5(\mathrm{I})}| < |u_{4(\mathrm{II})}|$. Thus, creating tetragonal tetramers (II) seems to be more favorable than creating pentagonal pentamers (I) to lower the total energy. In the simulations, however, pentagonal pentamers (I) are more numerous than tetragonal tetramers (II) when $\Delta/\sigma \geq 0.9$ and θ is 50° or 55°, which is probably because some of the nearest neighbors in pentagonal pentamers (I) are connected.

A hexagonal heptamer forms when one particle is included in the center of a ring-shaped hexagonal hexamer [(b6) in Figure 7(b)]. When Δ/σ is minimum, the minimum θ is the same as that of regular hexagonal hexamer. Since the center particle in the ideal hexagonal heptamer can interact with three other particles in the same cluster, the interaction energy change per particle for creating a hexagonal heptamer, u_7, is given by $-18\epsilon/7$. Since the minimum Δ necessary for creating hexagonal heptamers and hexagonal hexamers are same and $|u_6| < |u_7|$, the hexagonal heptamers should be created more easily than the regular hexagonal hexamers. However, the hexagonal hexamers are more numerous than the hexagonal heptamers. The hexagonal heptamers are created by adding particles in ideal regular hexagonal hexamers. As shown cluster (C) in Fig 4(c), the hexagonal hexamers are a bit deformed. To create the hexagonal heptamers, such deformations are not acceptable for the ring-shaped hexamer part in the heptamers. The hexagonal hexamer part is unstable because $\Delta/\sigma = 1$ is too short to keep its shape against thermal fluctuations. Thus, the number of the hexagonal heptamers appearing in our simulations is small.

To create long chain-like clusters formed by the connections of square clusters, Δ/σ should be larger than $(\sqrt{2}-1)$. With the minimum Δ, particle (E) can interact with particles (F), (J), and (K) in (b7) in Figure 7(b) when $\theta > 67.5^\circ$. When the effect of thermal fluctuations

is taken into account, the criterion of θ for creating long chain-like clusters seems to be satisfied because the chain-like clusters are numerous when $\theta \geq 75^\circ$ in my simulations. In Figure 1(f), the minimum Δ/σ for creating island-like clusters consisting of a square lattice with the lattice constant σ is also estimated to $(\sqrt{2}-1)$ because the particles in the diagonal positions need to be able to interact with each other. θ should be larger than 90° for the minimum Δ/σ. Even when θ is larger than the minimum value, there are non-interacting neighboring particles if the patch directions are parallel to the plane where particles are placed. However, all the neighboring particles can interact when the patch directions are perpendicular to the plane no matter whether the patch directions are same or opposite, which is because the path area is large enough for the particles with the opposite patch directions to interact with each other. Thus, the patch directions in the island-like clusters are perpendicular to the plane.

Dependence of cluster shape on $\epsilon/k_{\mathrm{B}}T$ and ϕ

Lastly, I study the dependence of cluster shape on $\epsilon/k_{\mathrm{B}}T$ and ϕ and show how the dependence of the type of the most numerous cluster on θ changes with these parameters.

Dependence of cluster shape on $\epsilon/k_{\mathrm{B}}T$. The dependence of the most numerous cluster on θ and Δ for $\epsilon/k_{\mathrm{B}}T = 4.0$ and 12.0 is shown in Figure 8. When the interaction energy is smaller than that in Figure 7 [Figure 8(a)], the parameter region where the dimer is the most numerous cluster spreads larger than that with $\epsilon/k_{\mathrm{B}}T = 8.0$. The parameter regions where square tetramers (I) and pentagonal pentamers (I) are the most numerous clusters do not appear. These results mean that tetramers (I) and pentamers (I) are more unstable than other polygonal clusters, which is probably because there are unconnected particles in tetramers (I) and pentamers (I). Since the parameter regions with other polygonal clusters shift to large θ direction, the area of the parameter region with chain-like clusters decreases, and the chain-like clusters becomes shorter than those with $\epsilon/k_{\mathrm{B}}T = 8$ as shown

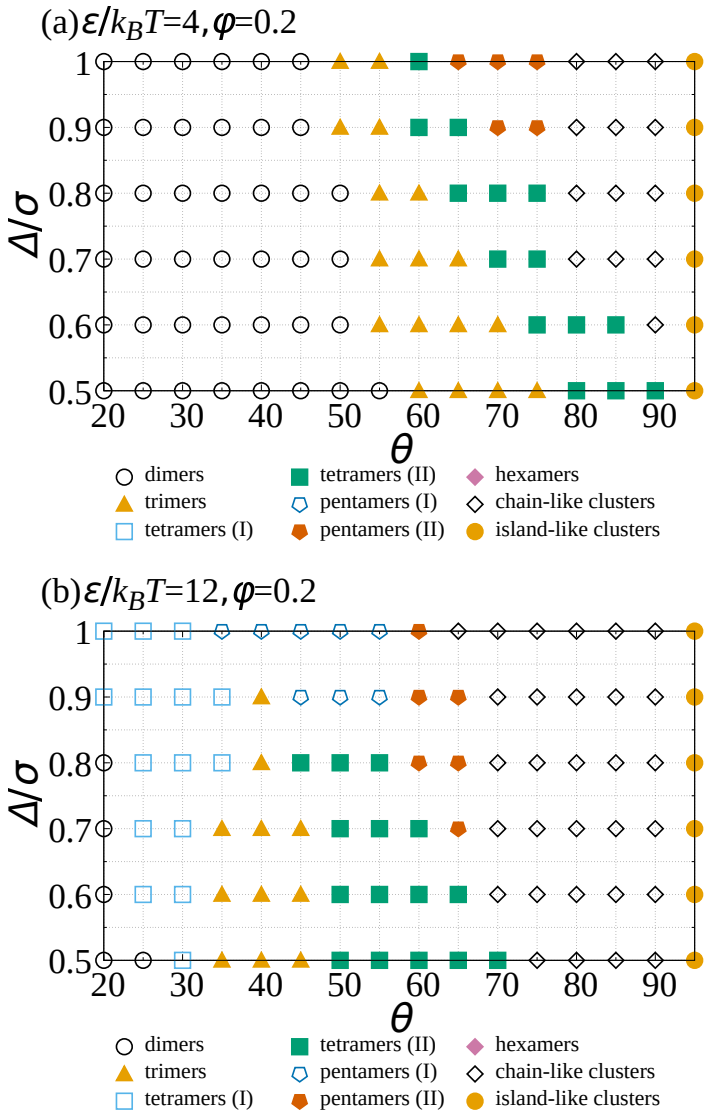

Figure 8: Dependence of the type of the most numerous cluster on θ and Δ for (a) $\epsilon/k_{\mathrm{B}}T = 4.0$ and (b) $\epsilon/k_{\mathrm{B}}T = 12.0$. $\phi = 0.2$ for both cases.

in Figure 9(a).

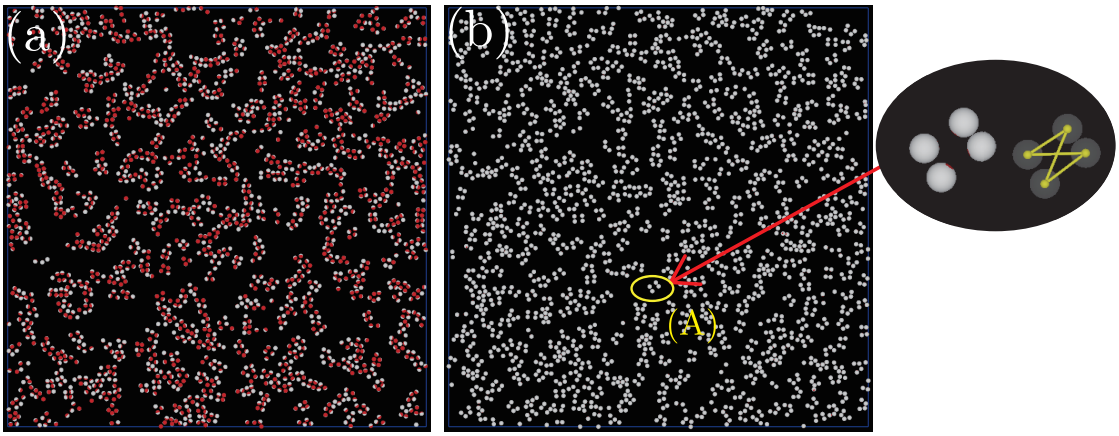

Figure 9: (a) Snapshot of a system with small chain-like clusters, where $\phi = 0.2$, $N = 2048$, and $\epsilon/k_{\mathrm{B}}T = 4.0$. Δ/σ and θ are 0.7 and 85°, and (b) Snapshot of a system and a zoomed snapshot of square tetramers (I), where $\phi = 0.2$, $N = 2048$, and $\epsilon/k_{\mathrm{B}}T = 12.0$. Δ/σ and θ are 1.0 and 20°, respectively.

When $\epsilon/k_{\mathrm{B}}T = 12.0$ [Figure 8(b)], tetragonal tetramers (I) and pentagonal pentamers (I) are created, which is similar to systems with $\epsilon/k_{\mathrm{B}}T = 8.0$. The region with tetramers (I) is larger than that with $\epsilon/k_{\mathrm{B}}T = 8.0$. When $\Delta/\sigma \geq 0.9$, tetramers (I) form even with $\theta = 20°$, which is smaller than the minimum θ for forming regular square tetramers (I) with the minimum Δ/σ. The formation of tetramers (I) in the small θ region is caused by the deformation of the cluster shape. Figure 9(b) shows a snapshot of a system with $\theta = 20°$ and a zoomed snapshot of a deformed tetramer (I). Since its shape seems to be rectangular rather than square, the angle formed by a connected nearest neighbor and the particle in the diagonal position is small, which makes the formation of tetramers (I) with small θ possible.

Dependence of cluster shape on ϕ. The dependence of the types of the most numerous clusters on θ and Δ for $\phi = 0.1$ and $\phi = 0.3$ is shown in Figure 10. When $\phi = 0.1$ [Figure 10(a)], the region where chain-like clusters are dominant becomes smaller than that with $\phi = 0.2$. On the contrary, when $\phi = 0.3$ [Figure 10(a)], the region where chain-like clusters are the most numerous clusters becomes larger than that with $\phi = 0.2$. Compared with the changes in the dependence of the types of the most numerous clusters, which is

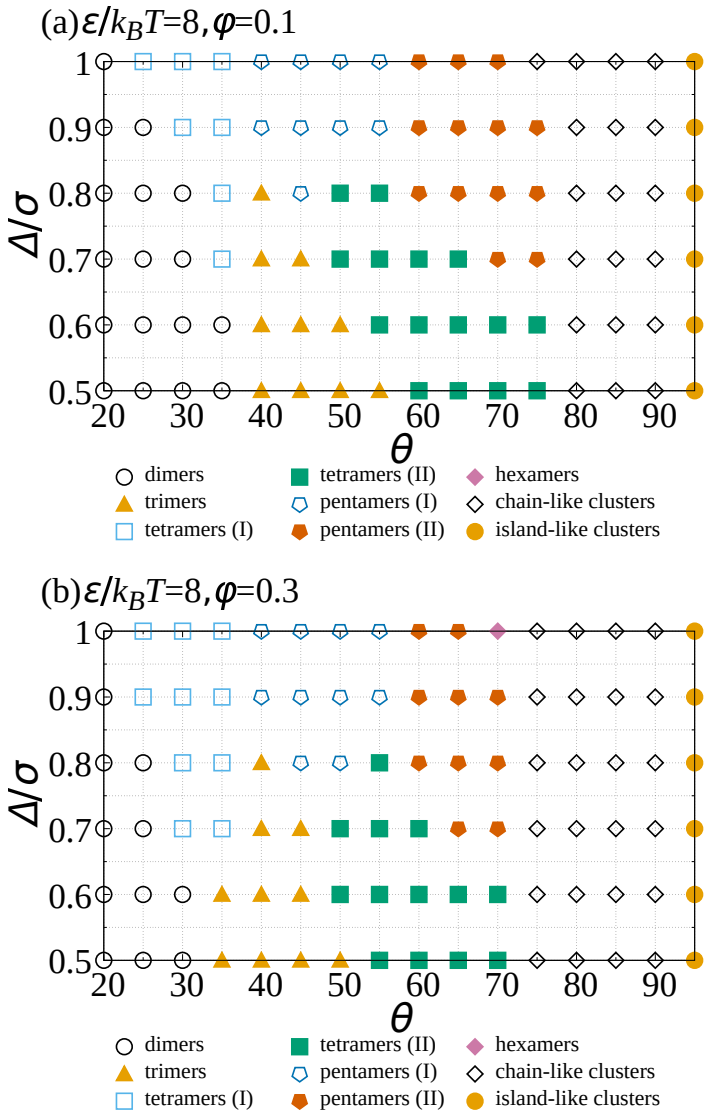

Figure 10: Dependence of the type of the most numerous cluster on θ and Δ for (a) $\phi = 0.1$ and (b) $\phi = 0.3$. $\epsilon/k_{\mathrm{B}}T = 8.0$ for both cases.

induced by the difference in the interaction energy (Figure 8), the changes in the parameter regions induced by the difference in the particle density are small in these causes. Thus, the parameters which mainly determine cluster shape are the interaction energy, the interaction length, and the interaction width. The dependence of the type of the most numerous cluster on ϕ is small if the particle density is not too large.

Conclusions

In this paper, I performed isothermal-isochoric Monte Carlo simulations and study the clusters formed by one-patch particles. I studied the possibility of formation of various types of clusters for $\Delta/\sigma \geq 0.5$, which is longer than that in previous studies,[7,16,18,20,26,46] focusing on the cluster formation in two-dimensional systems because structures and clusters in these systems were interested as functional materials.[42,43] I considered that one-patch particle rotate three-dimensionally and translate on a two-dimensional flat plane. The KF potential was used as the potential between the spherical patchy particles, and the dependence of the two-dimensional self-assemblies on the patch area and interaction length were examined.

In previous studies,[18,20] chain-like clusters are created in the three-dimensional systems when the patch area is small. The unit of the chain-like clusters are a dimer or a trimer because interaction length is short. In my simulations, I found that regular polygonal clusters such as square tetramers, pentagonal pentamers, hexagonal hexamers, and hexagonal heptamers are created for long-range interaction. When we use those polygonal clusters as building blocks, we may be able to create chain-like clusters whose unit is square tetramers or larger polygonal clusters. When the patch area is large, bilayers are created in the three-dimensional systems. The lattice structures in their sheets is a triangular lattice when $\Delta/\sigma < 0.5$.[18,46] However, since island-like clusters with square lattice form with $\Delta/\sigma > 0.5$, it may be possible to create the bilayers with square lattice when the interaction length Δ/σ is long.

Acknowledgement

This work was supported by JSPS KAKENHI Grants, Nos. JP20K03782, JP18K04960, and JP18H03839, and the Grant for Joint Research Program of the Institute of Low Temperature Science, Hokkaido University, Grant number 20G029.

References

(1) Ho, K. M.; Chan, C. T.; Soukoulis, C. M. Existence of a Photonic Gap in Periodic Dielectric Structures. *Phys. Rev. Lett.* **1990**, 65, 3152 − 3155.

(2) Maldovan, M.; Thomas, E. L. Diamond-structured Photonic Crystals. *Nat. Mater.* **2004**, 3, 593 − 600.

(3) Morphew, D.; Neophytou, A.; Avins, C.; Chakrabarti, D. Programming Hierarchical Self-Assembly of Patchy Particles into Colloidal Crystals via Colloidal Molecules. *ACS Nano* **2018**, 14, 2355-2364.

(4) Rao, A. B.; Shaw, J.; Neophytou, A.; Morphew, D.; Sciortino, F.; Johnston, R. L..; Chakrabarti, D. Leveraging Hierarchical Self-Assembly Pathways for Realizing Colloidal Photonic Crystals. *ACS Nano* **2020**, 14, 5348-5359.

(5) Zhang, Z.; Keys, A. S.; Chen, T.; Glotzer, S. C. Self-Assembly of Patchy Particles into Diamond Structures through Molecular Mimicry *Langmuir* **2005**, 21, 11547-11551.

(6) Bianchi, E.; Largo, J.; Tartaglia, P.; Zaccarelli, E.; Sciortino, F. Phase Diagram of Patchy Colloids: Towards Empty Liquids. *Phys. Rev. Lett.* **2006**, 97, 168301.

(7) Hong, L.; Cacciuto, A.; Luijten, E.; Granick, S. Clusters of Amphiphilic Colloidal Spheres. *Langmuir* **2008**, 24, 621-625.

(8) Miller, W. L.; Cacciuto, A. Hierarchical self-assembly of asymmetric amphiphatic spherical colloidal particles. *Phys. Rev. E:Stat., Nonlinear, Soft Matter Phys.* **2009**, 80, 021404.

(9) Pawar A. B.; Kretzschmar, I. Patchy Particles by Glancing Angle Deposition *Langmuir* **2008**, 24, 355-358.

(10) Sciortino, F.; Giacometti, A.; Pastore, G. Phase Diagram of Janus Particles. *Phys. Rev. Lett.* **2009**, 103, 237801.

(11) Chen, Q.; Bae, S. C.; Granick, S. Directed self-assembly of a colloidal kagome lattice. *Nature* **2011**, 469, 381-384.

(12) Chen, Q.; Yan, J.; Zhang, J.; Bae, S. C.; Granick, S. Janus and Multiblock Colloidal Particles. *Langmuir* **2012**, 28, 13555-13561.

(13) Romano, F.; Sanz, E.; Tartaglia, P.; Sciortino, F. Phase diagram of trivalent and pentavalent patchy particles. *J. Phys.: Condens. Matter* **2012**, 24, 064113.

(14) Romano, F.; Sciortino, F. Patterning symmetry in the rational design of colloidal crystals. *Nat. Commun.* **2012**, 3, 975.

(15) Wang, Y.; Wang, Y.; Breed, D. R.; Manoharan, V. N.; Feng, L.; Hollingsworth, A. D.; Weck, M.; Pine. D. J. Colloids with valence and specific directional bonding. *Nature* **2012**, 491, 51-55.

(16) Iwashita, Y.; Kimura, Y. Stable cluster phase of Janus particles in two dimensions. *Soft Matter* **2013**, 9, 10694-10698.

(17) Mao, X.; Chen, Q.; Granick, S. Entropy favours open colloidal lattices. *Nat. Mat.* **2013**, 12, 217-222.

(18) Preisler, Z.; Vissers, T.; Smallenburg, F.; Munaò, G; Sciortino, F. Phase Diagram of One-Patch Colloids Forming Tubes and Lamellae. *J. Phys. Chem. B* **2013**, 117, 9540-9547.

(19) Vissers, T.; Preisler, Z.; Smallenburg, F.; Dijkstra, M.; Sciortino, F. Predicting crystals of Janus colloids. *J. Chem. Phys.* **2013**, 138 164505.

(20) Vissers, T.; Smallenburg, F.; Munaò, G.; Preisler, Z.; Sciortino, F. Cooperative polymerization of one-patch colloids. *J. Chem. Phys.* **2014**, 140, 144902.

(21) Shah, A. A.; Schultz, B.; Kohlstedt, K. L.; Glotzer, S. C.; Solomon, M. J. Synthesis, Assembly, and Image Analysis of Spheroidal Patchy Particles *Langmuir* **2013**, 29, 4688-4696.

(22) Iwashita, Y.; Kimura, Y. Orientational order of one-patch colloidal particles in two dimensions. *Soft Matter* **2014**, 10, 7170-7181.

(23) Shin, H.; Schweizer, K. S. Theory of two-dimensional self-assembly of Janus colloids: crystallization and orientational ordering. *Soft Matter* **2014**, 10, 262-274.

(24) Preisler, Z.; Vissers, T.; Munaò, G.; Smallenburg, F.; Sciortino, F. Equilibrium phases of one-patch colloids with short-range attractions. *Soft Matter* **2014**, 10, 5121-5128.

(25) Iwashita, Y.; Kimura, Y. Spatial confinement governs orientational order in patchy particles. *Sci. Rep.* **2016**, 6, 27599.

(26) Preisler, Z.; Vissers, T.; Smallenburg, F.; Sciortino, F. Crystals of Janus colloids at various interaction ranges. *J. Chem. Phys.* **2016**, 145, 064513.

(27) Reinhart, W. F.; Panagiotopoulos, A. Z. Equilibrium crystal phases of triblock Janus colloids. *J. Chem. Phys.* **2016**, 145, 094505.

(28) Gong, Z.; Hueckel, T.; Yi, G.-R.; Sacanna, S. Patchy particles made by colloidal fusion. *Nature* **2017**, 550, 234-238.

(29) Zhang, J.; Grzybowski, B. A.; Granick, S. Janus Particle Synthesis, Assembly, and Application *Langmuir* **2017**, 33, 6964-6977.

(30) Bianchi, E.; van Oostrum, P. D. J.; Likos, C. N.; Kahl G. Inverse patchy colloids: Synthesis, modeling and self-organization. *Curr. Opin. Colloid Interface Sci.* **2017**, 30, 8-15.

(31) Iwashita, Y.; Kimura, Y. Density dependence of orientational order in one-patch particles. *Soft Matter* **2017**, 13, 4997-5007.

(32) Patra N.; Tkachenko, A. V. Layer-by-layer assembly of patchy particles as a route to nontrivial structures. *Phys. Rev. E:Stat., Nonlinear, Soft Matter Phys.* **2017**, 96, 022601.

(33) Ravaine, S.; Duguet E. Synthesis and assembly of patchy particles: Recent progress and future prospects. *Curr. Opin. Colloid Interface Sci.* **2017**, 30, 45-53.

(34) Jalilvand, Z.; Pawar, A. B.; Kretzschmar, I. Experimental Study of the Motion of Patchy Particle Swimmers Near a Wall *Langmuir* **2018** 34, 15593-15599

(35) Reinhart, W. F.; Panagiotopoulos, A. Z. Directed assembly of photonic crystals through simple substrate patterning. *J. Chem. Phys.* **2019** 150, 014503

(36) Cerbelaud, M.; Lebdioua, K.; Tran, C. T.; Crespin, B.; Aimablea, A.; Videcoqa, A. Brownian dynamics simulations of one-patch inverse patchy particles. *Phys. Chem. Chem. Phys.* **2019**, 21, 23447–23458.

(37) Noguchi, T. G; Iwashita, Y.; Kimura, Y. Controlled armoring of metal surfaces with metallodielectric patchy particles. *J. Chem. Phys.* **2019**, 150, 174903.

(38) Oh, J. S.; Lee, S.; Glotzer, S. C.; Yi, G.-R.; Pine, D. J. Colloidal fibers and rings by cooperative assembly. *Nat. Commun.* **2019**, 10, 3936.

(39) A, J. A. D.; Oh, J. S.; Yi, G.-R.; Pine, D. J. Photo-printing of faceted DNA patchy particles *Proc. Natl. Acad. Sci. U.S.A.* **2020**, 1170, 10645-10653.

(40) Oh, J. S.; Yi, Gi-R; Pine, D. J. Reconfigurable Transitions between One- and Two-Dimensional Structures with Bifunctional DNA-Coated Janus Colloids *ACS Nano* **2020**, 14, 15786 − 15792.

14, 5348-5359.

(41) Kamp, M.; de Nijs, B.; van der Linden, M. N.; de Feijter, I.; Lefferts, M. J.; Aloi, A.; Griffiths, J.; Baumberg, J. J.; Voets, I. K.; van Blaaderen A. Multivalent Patchy Colloids for Quantitative 3D Self-Assembly Studies *Langmuir* **2020**, 36, 2403 − 2418.

(42) Dong, R.; Zhang,T.; Feng, X. 2D nanomaterials: beyond graphene and transition metal dichalcogenides. *Chem. Rev.* **2018**, 118, 6189-6235.

(43) Wang, H.; Liux, X.; Niu, P.; Wang,S.; Shi, J.; Li, L. Porous Two-Dimensional Materials for Photocatalytic and Electrocatalytic Applications. *Matter* **2020**, 2, 1377-1413.

(44) Kern, N.; Frenkel, D. Fluid-fluid coexistence in colloidal systems with short-ranged strongly directional attraction. *J. Chem. Phys.* **2003**, 118, 9882.

(45) Sato, M. Self-Assembly Formed by Spherical Patchy Particles with Long-Range Attraction. *J. Phys. Soc. Jpn* **2019**, 88, 104801.

(46) Sato, M. Effect of Patch Area and Interaction Length on Clusters and Structures Formed by One-Patch Particles in Thin Systems *ACS Omega* **2020**, 5, 28812 − 28822

(47) van Blaaderen, A.; Ruel, R.; Wiltzius, P. Template-directed colloidal crystallization. *Nature* **1997**, 385, 321-324.

(48) Lin, K.-h.; Crocker, J. C.; Prasad, V.; Schofield, A., Weitz, D. A.; Lubensky, T. C.; Yodh, A. G. Entropically Driven Colloidal Crystallization on Patterned Surfaces. *Phys. Rev. Lett.* **2000**, 85, 1770.

(49) Savage, J. R.; Hopp, S. F.; Ganapathy, R.; Schofield Gerbode, S. J.; Heuer, A.; Cohen, I. Entropy-driven crystal formation on highly strained substrates. *Proc Natl Acad Sci U S A.* **2013**, 110, 9301-9304.

(50) Mirkin, C. A.; Letsinger, R. L; Mucic, R. C.; Storhoff, J. J. A DNA-based method for rationally assembling nanoparticles into macroscopic materials *Nature* **1996**, 382, 607-609.

(51) Nykypanchuk, D.; Maye, M. M.; van der Lelie, D. ; Gang, O. DNA-guided crystallization of colloidal nanoparticles. *Nature* **2008**, 451, 549-552.

(52) Park, S. Y.; Lytton-Jean, A. K. R.; Lee, B.; Weigand, S.; Schatz, G. C.; Mirkin, C. A. DNA-programmable nanoparticle crystallization. *Nature* **2008**, 451, 553-556.

(53) Xiong, H.; Lelie, D. v. d.; Gang O. Phase Behavior of Nanoparticles Assembled by DNA Linkers. *Phys. Rev. Lett.* **2009**, 102, 015504.

(54) Macfarlane, R. J.; Lee, B.; Hill, H. D.; Senesi, A. J.; Seifert, S.; Mirkin, C. A. Assembly and organization processes in DNA-directed colloidal crystallization. *Proc. Natl. Acad. Sci. U.S.A.* **2009**, 106, 10493-10498.

(55) Jones, M. R.; Macfarlane, R. J. ; Lee, B.; Zhang, J.; Young, K. L.; Senesi, A. J.; Mirkin, C. A. DNA-nanoparticle superlattices formed from anisotropic building blocks. *Nat. Mater.* **2010**, 9 ,913-917.

(56) Cigler, P.; Lytton-Jean, A. K. R.; Anderson, D. G.; Finn, M. G.; Park, S. Y. DNA-controlled assembly of a NaTl lattice structure from gold nanoparticles and protein nanoparticles. *Nat. Mater.* **2010**, 9 ,918-922.

(57) Macfarlane, R. J.; Lee. B.; Jones, M. R.; Harris, N.; Schatz, G. C. ; Mirkin, C. A. Nanoparticle Superlattice Engineering with DNA. *Science* **2011**, 334, 204-208.

(58) Knorowski, C.; Burleigh, S.; Travesset, A. Dynamics and Statics of DNA-Programmable Nanoparticle Self-Assembly and Crystallization. *Phys. Rev. Lett.* **2011**, 106, 215501.

(59) Rogers, W. B,; Crocker, J. C. Direct measurements of DNA-mediated colloidal interactions and their quantitative modeling. *Proc. Natl. Acad. Sci. U.S.A.* **2011**, 108, 15687-15692.

(60) Zhang, C.; Macfarlane, R. J.; Young, K. L.; Choi, C. H. J.; Hao, L.; Auyeung, E.; Liu, G.; Zhou, X,; Mirkin, C. A. A general approach to DNA-programmable atom equivalents. *Nat. Mater.* **2013**, 12, 741-746.

(61) Li, T. I. N. G.; Sknepnek, R.; de la Cruz, M. O. Thermally Active Hybridization Drives the Crystallization of DNA-Functionalized Nanoparticles. *J. Am. Chem. Soc.* **2013**, 135, 8535-8541.

(62) Di Michele, L.; Varrato, F.; Kotar, J.; Nathan, S. H.; Foffi, G.; Eiser, E. Multistep kinetic self-assembly of DNA-coated colloids. *Nat. Commun.* **2013**, 4, 2007.

(63) Srivastava, S.; Nykypanchuk, D.; Fukuto, M,; Halverson, J. D.; Tkachenko, A. V.; Yager, K. G.; Gang, O. Two-Dimensional DNA-Programmable Assembly of Nanoparticles at Liquid Interfaces.*J. Am. Chem. Soc.* **2014**, 136, 8323-8332.

(64) Isogai, T.; Akada E.; Nakada, S.; Yoshida, N.; Tero, R.; Harada, S.; Ujihara, T.; Tagawa, M. Effect of magnesium ion concentration on two-dimensional structure of DNA-functionalized nanoparticles on supported lipid bilayer. *Jpn. J. Appl. Phys.* **2016**, 55, 03DF11.

(65) Katsuno, H.; Maegawa, Y.; Sato, M. Two-Dimensional Crystal Structure Formed by Two Components of DNA Nanoparticles on a Substrate. *J. Phys. Soc. Jpn* **2016**, 85, 074605.

(66) Pretti, E.; Zera, H.; Song, M.; Ding, Y.; Mahynski, N. A.; Hatch, H. W.; Shen, V. K.; Mittal, J. Assembly of three-dimensional binary superlattices from multi-flavored particles. *Soft Matter* **2018**, 14, 6303-6312.

(67) Wang, S.; Park, S. S.; Buru, C. T.; Lin, H.; Chen, P.-C.; Roth, E. W.; Farha, O. K.; Mirkin, C. A. Colloidal crystal engineering with metal-organic framework nanoparticles and DNA. *Nat. Commun.* **2020**, 11, 2495.

(68) Sato, M. Two-dimensional structures formed in a binary system of DNA nanoparticles with a short-range interaction potential. *Jpn. J. Appl. Phys.* **2018**, 57, 125002.

Table of Contents Graphic